Supplement of Hydrol. Earth Syst. Sci., 30, 5473–5490, 2026
https://doi.org/10.5194/hess-30-5473-2026-supplement

Hydrology and Earth System Sciences
Open Access

Supplement of

Impacts of cascading check dams on sediment yield in the Middle Yellow River Basin: insights from 50 years of grid-cell-level simulation

Yanzhang Huang et al.

Correspondence to: Guangyao Gao (gygao@rcees.ac.cn)

Contents of this file

Sections S1 to S2

Figures S1 to S12

Tables S1 to S2

Introduction

The sections include the description for NDVI data harmonization method (Section S1) and the description for the trade-off analysis method between sediment reduction contribution and sediment accumulation amount of check dams (Section S2). The figures include the accuracy evaluation of the corrected GIMMS NDVI using MOD13Q1 NDVI (Figure S1), parameter calibration results of IC_0 and K_{IC} for each sub-basin (Figure S2), the comparison between simulated and measured sediment storage in check dams (Figure S3), the temporal and spatial results of soil erosion (Figures S4 and S5), the results of the intermediate parameters IC and SDR used to calculate sediment yield (Figures S6 and S7), the spatial distribution and temporal changes in the sediment trapping efficiency of check dams (Figure S8), detailed sediment-yield maps after accounting for sediment interception (Figure S9), the temporal dynamics of sediment reduction contribution and sediment deposition across sub-basins (Figures S10 and S11), and sensitivity of simulated sediment accumulation in check dams to different values of the empirical coefficient *D* in calculating sediment trapping efficiency (Figure S12). The tables provide basic information for the 17 hydrological stations (Table S1) and the empirical assignment scheme for the *P* factor in the RUSLE model (Table S2).

Section S1. NDVI data harmonization

To construct a consistent long-term NDVI time series, the GIMMS-NDVI-3g and MOD13Q1 datasets were harmonized during their overlapping period from 2000 to 2015 using spatiotemporal stability assessment and statistical downscaling (Huang et al., 2024). First, the GIMMS NDVI data were resampled to the same spatial resolution as the MODIS data. Because vegetation phenology and physiological conditions differ among months, pixel-wise regression relationships between GIMMS NDVI at 250 m resolution and MODIS NDVI at 250 m resolution were established separately for each month from January to December. The corresponding regression parameters were then obtained for each pixel. These regression equations were used to correct the GIMMS NDVI data and assimilate them with the MODIS NDVI dataset. The corrected GIMMS NDVI during the overlapping period was further compared with MODIS NDVI (Fig. S1). Finally, the corrected GIMMS NDVI before March 2000 and MODIS NDVI after March 2000 were combined to generate the GIMODIS NDVI dataset.

Section S2. Trade-off analysis method between sediment reduction contribution and sediment accumulation amount of check dams

Bradford and D'Amato (2012) have elucidated a straightforward approach for quantifying the consequences of different management scenarios based on the trade-offs and benefits among multiple objectives. This method has been widely employed in balancing two or more management objectives (Chen et al., 2022; Langner et al., 2017; Su et al., 2021). We initially standardized the sediment reduction contribution of check dams (SRC_{dam}) and the proportion of accumulated sediment relative to total reservoir capacity (i.e., sediment accumulation ratio, SAR_{dam}) to eliminate the dimensional relationship between variables. The standardized environmental variables, also regarded as the relative benefits of environmental variables, are defined as (Bradford and D'Amato, 2012):

$$X_{std} = (X_{obs} - X_{min})/(X_{max} - X_{min}) \quad \text{(S1)}$$

where X_{std} is the standardized value of a management objective, X_{obs} is the observation value of the management objective, X_{min} and X_{max} are the minimum and maximum value of the management objective. Overall benefit is calculated as the mean of individual benefits and increases from low benefit in the lower left to greater benefit in the upper right (Bradford and D'Amato, 2012). Trade-off is calculated as the root mean squared error of the individual benefits and increases with distance from the 1:1 line.

References

Bradford, J. B. and D'Amato, A. W.: Recognizing trade-offs in multi-objective land management, Front. Ecol. Environ., 10, 210–216, https://doi.org/10.1890/110031, 2012.

Chen, Y., Wei, T., Ren, K., Sha, G., Guo, X., Fu, Y., and Yu, H.: The coupling interaction of soil organic carbon stock and water storage after vegetation restoration on the Loess Plateau, China, J. Environ. Manage., 306, 114481, https://doi.org/10.1016/j.jenvman.2022.114481, 2022.

Huang, Y., Xin, Z., Gao, G., Lu, X., Ran, L., Wang, Y., and Zhang, Z.: Increasing lateral transport of soil and carbon on the Tibetan Plateau, Catena, 239, 107901, https://doi.org/10.1016/j.catena.2024.107901, 2024.

Langner, A., Irauschek, F., Perez, S., Pardos, M., Zlatanov, T., Öhman, K., Nordström, E. M., and Lexer, M. J.: Value-based ecosystem service trade-offs in multi-objective management in

European mountain forests, Ecosyst. Serv., 26, 245–257, https://doi.org/10.1016/j.ecoser.2017.03.001, 2017.

Su, B., Su, Z., and Shangguan, Z.: Trade-off analyses of plant biomass and soil moisture relations on the Loess Plateau, Catena, 197, 104946, https://doi.org/10.1016/j.catena.2020.104946, 2021.

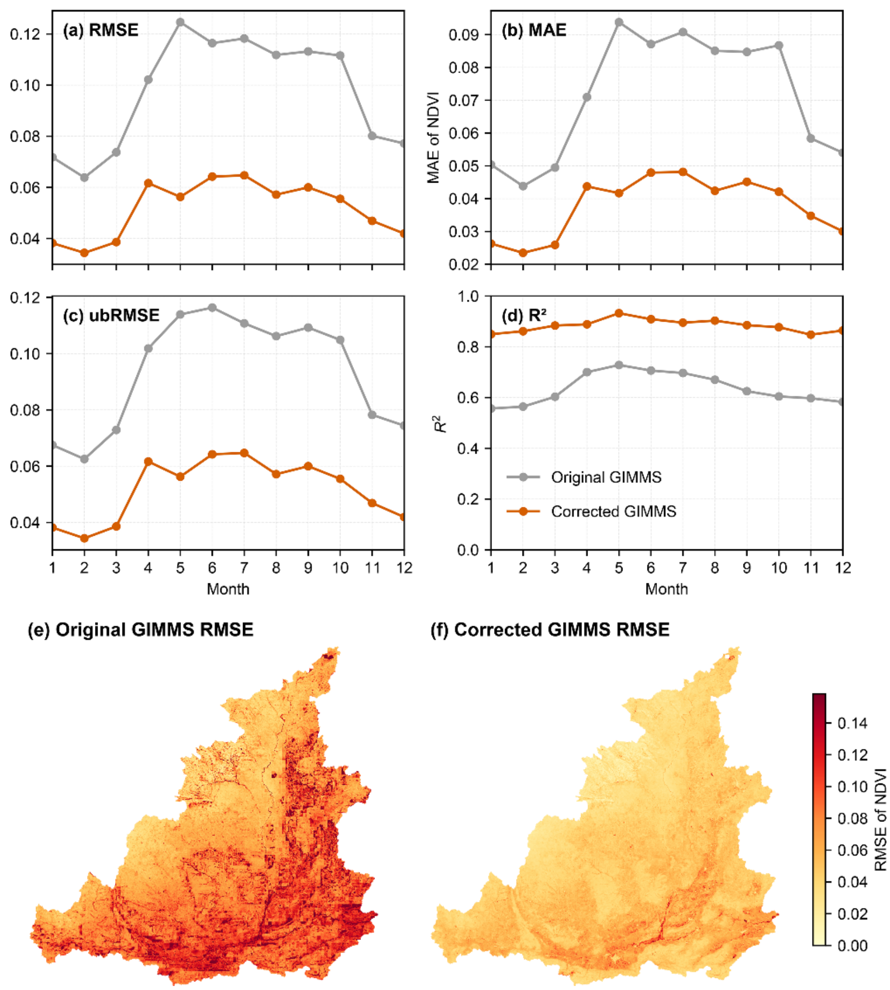

Figure S1. Accuracy evaluation of the corrected GIMMS-NDVI-3g using MOD13Q1 as the reference during the overlapping period (2000-2015). Panels (a–d) show the monthly variations in four accuracy metrics between GIMMS-NDVI-3g and MOD13Q1: root mean square error (*RMSE*), mean absolute error (*MAE*), unbiased root mean square error (*ubRMSE*), and coefficient of determination (R^2). Panels (e–f) show the spatial distribution of pixel-wise *RMSE* for the original and corrected GIMMS-NDVI-3g, respectively.

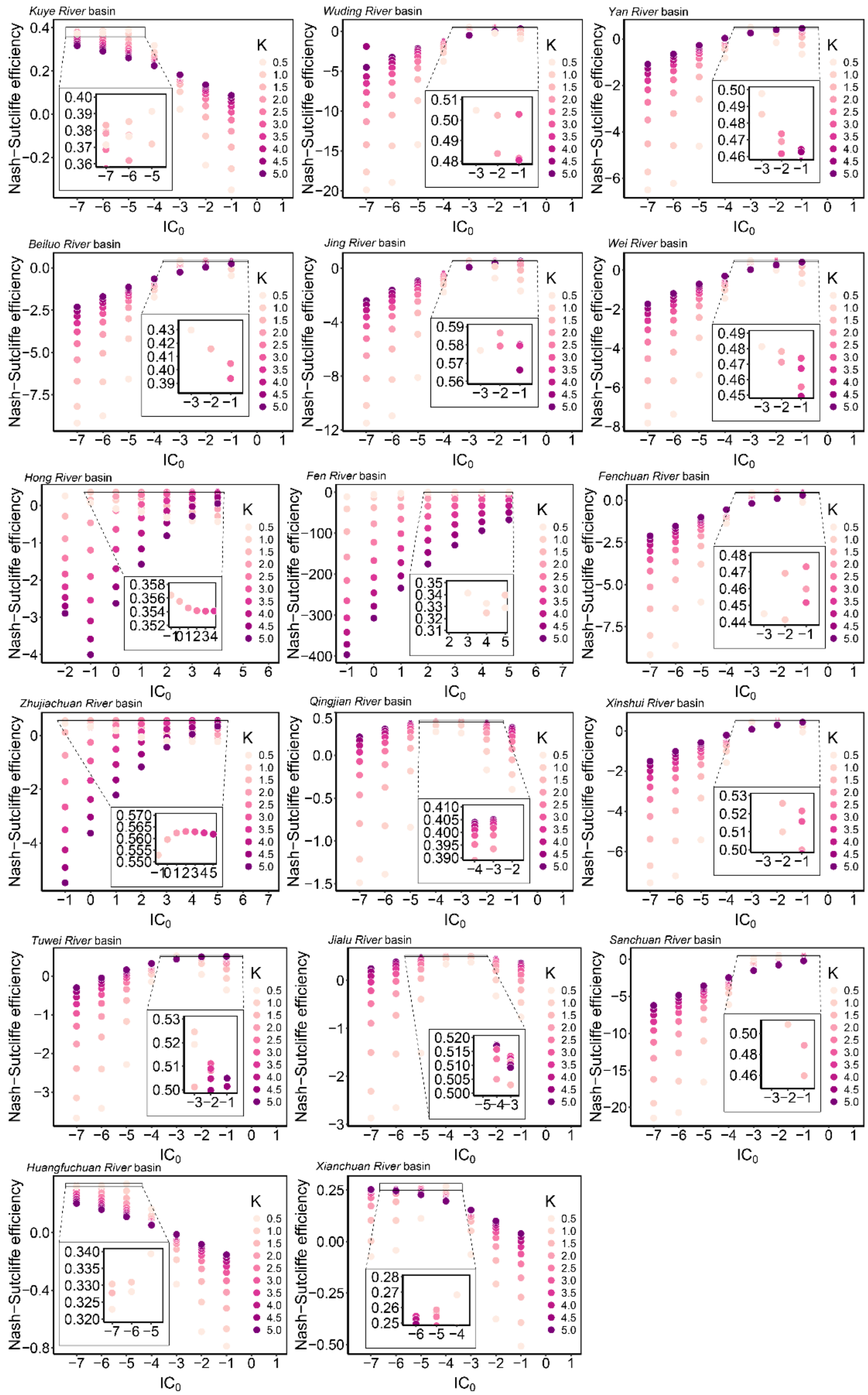

Figure S2. Calibration of IC_0 and K_{IC} parameter combinations for 17 sub-basins in the middle Yellow River Basin. The detailed inset reveals the optimal parameter combinations.

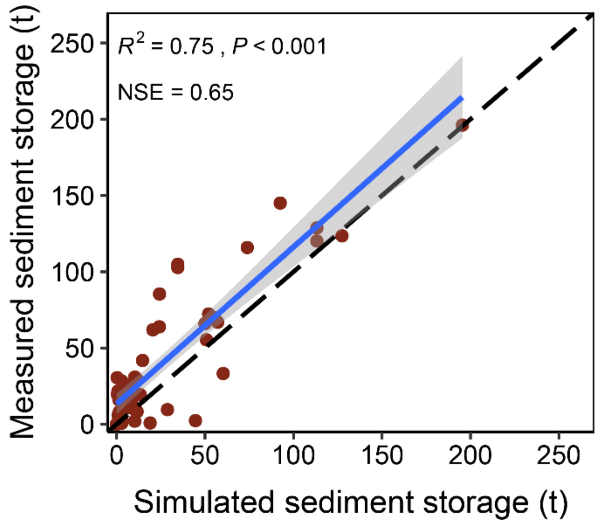

Figure S3. Comparison between simulated and measured sediment storage in check dams reported by Fang et al. (2023) (n=61). The dashed line indicates the 1:1 line, and the shaded area represents the 95% confidence interval of the fitted regression.

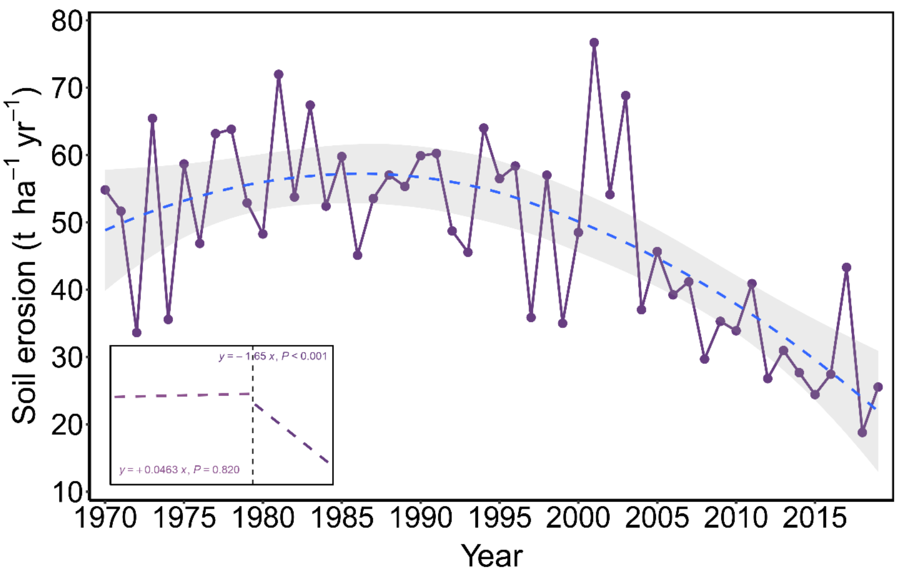

Figure S4. Interannual variations in average soil erosion rate of the middle Yellow River Basin from 1970 to 2020. The inset in the lower left displays the linear regression of soil erosion rate before and after 2001. The dashed line represents a fitted curve with the shaded area indicating the 95% confidence interval.

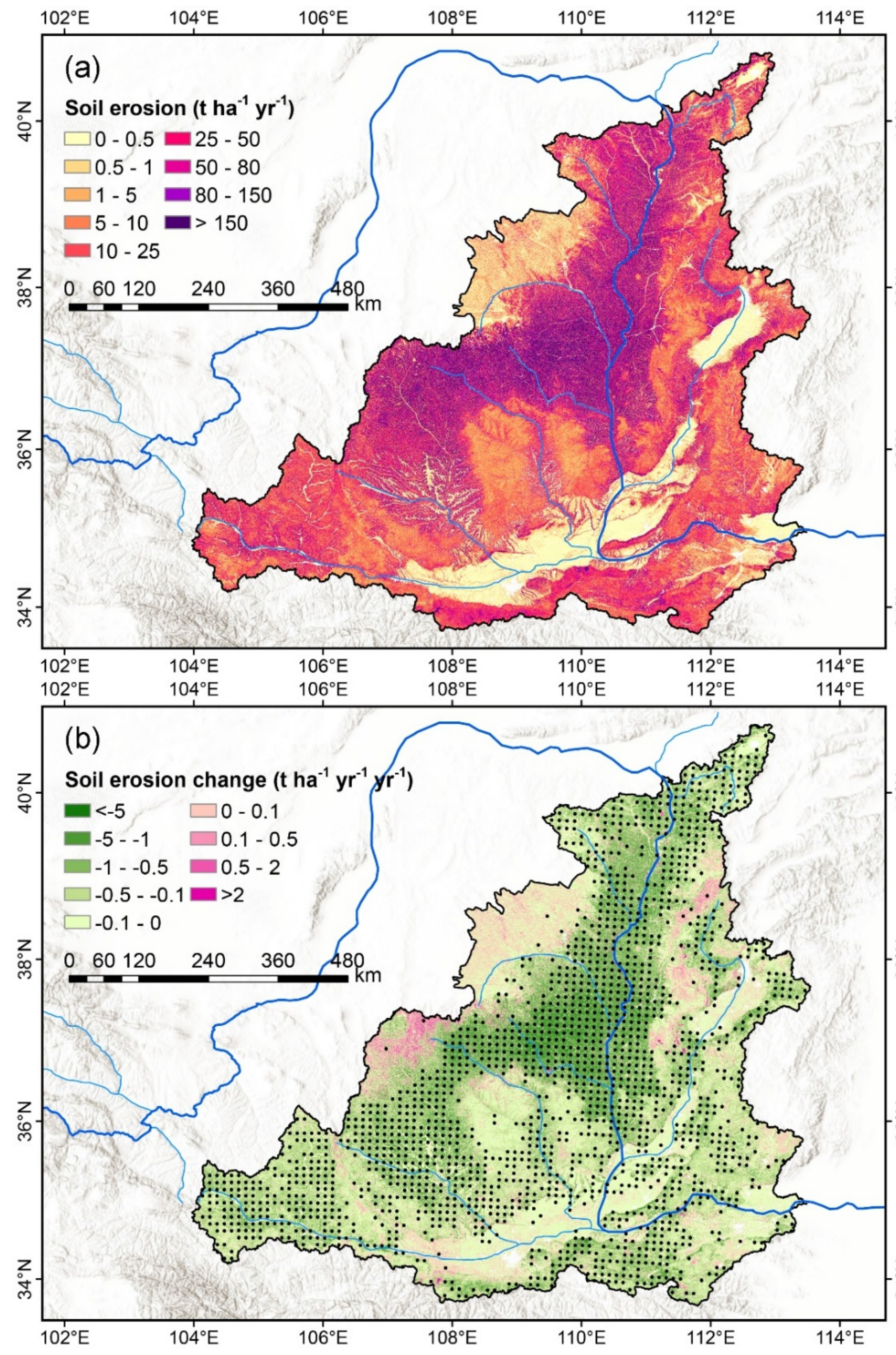

Figure S5. Spatial distribution of (a) average soil erosion during 1970-2020 and (b) soil erosion change over the 50-year period in the middle Yellow River Basin. Black dots in (b) mark areas with significant changes in soil erosion ($P < 0.05$).

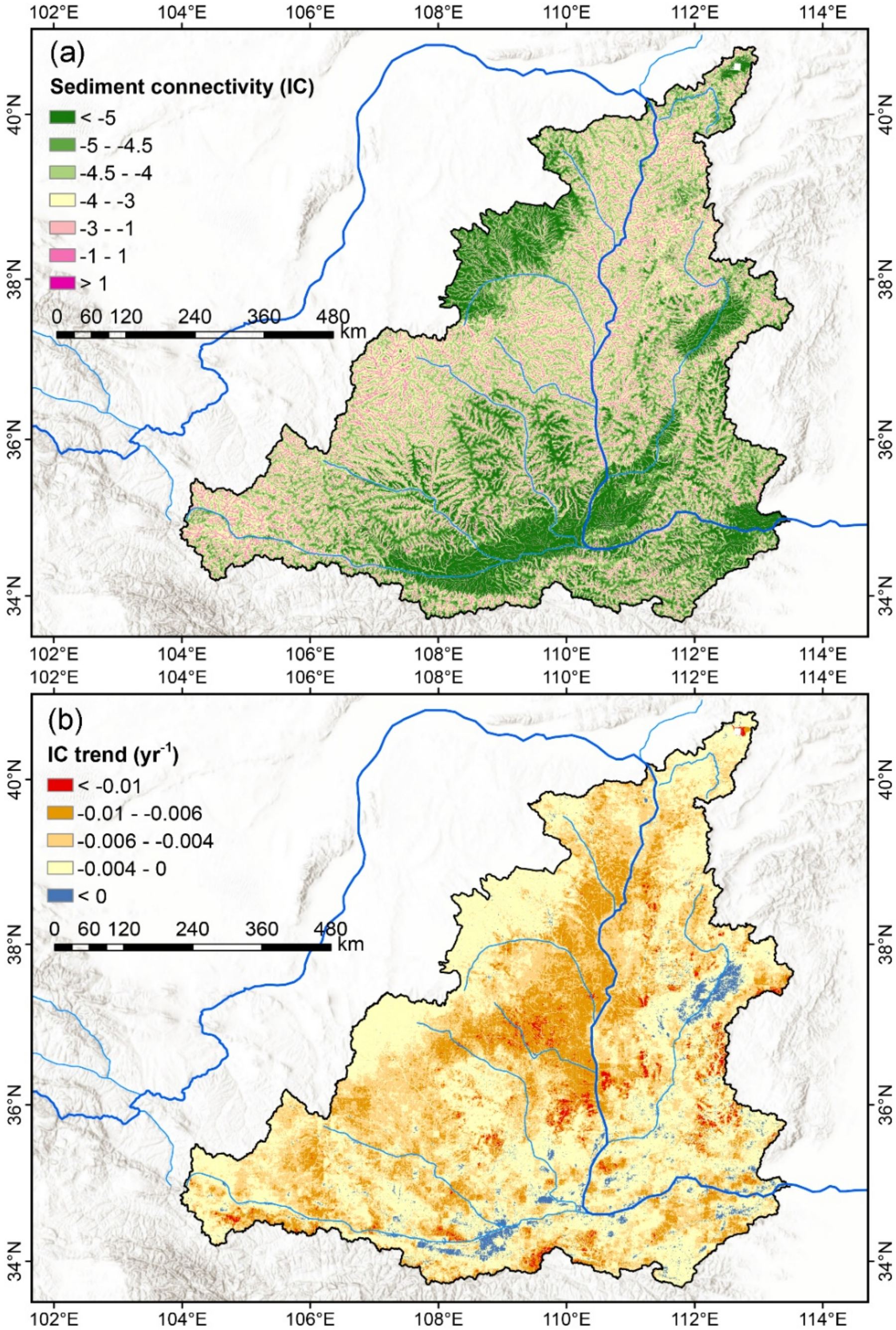

Figure S6. Spatial distribution of (a) average sediment connectivity (IC) during 1970-2020 and (b) trends of IC over the 50-year period in the middle Yellow River Basin.

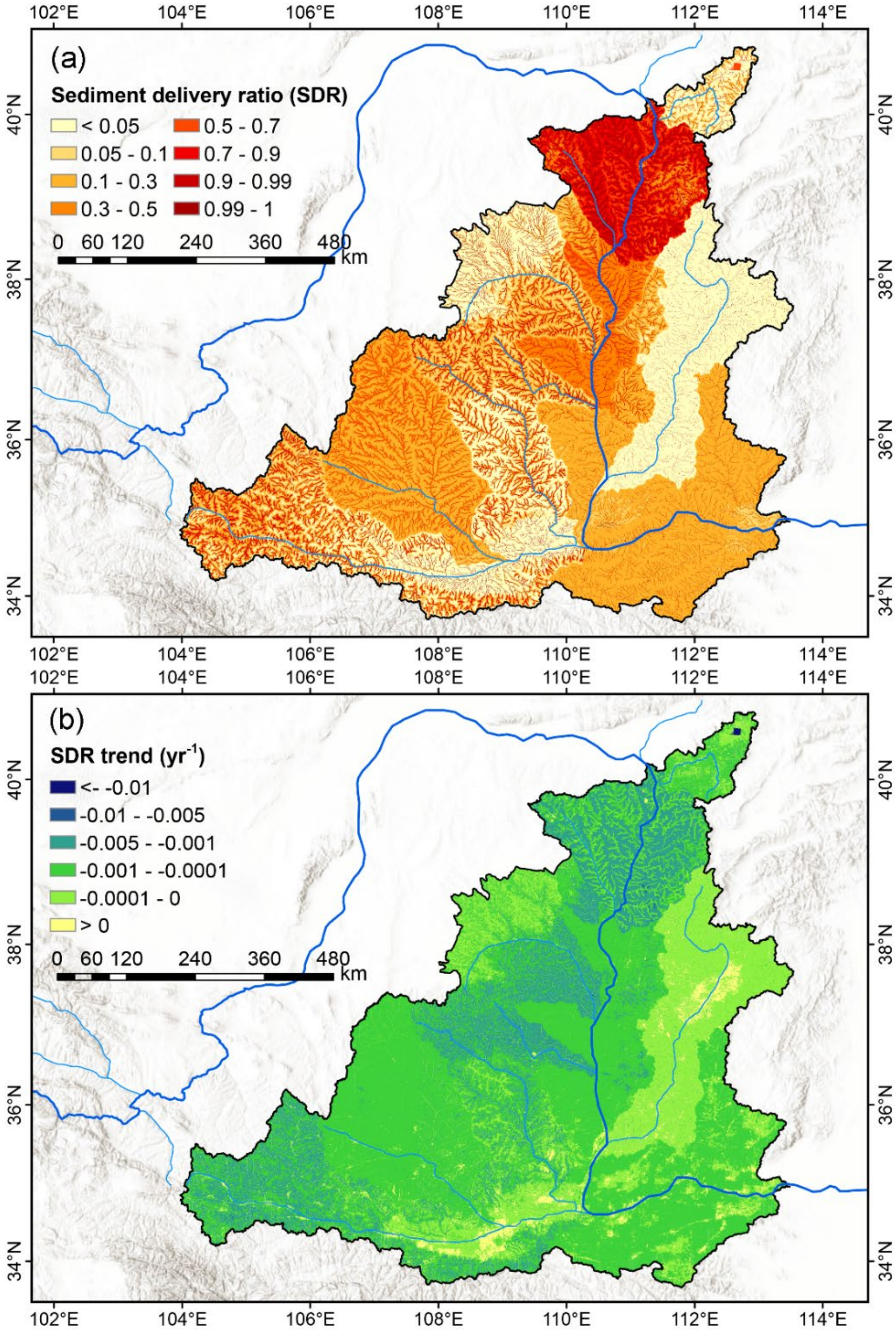

Figure S7. Spatial distribution of (a) average sediment delivery ratio (SDR) during 1970-2020 (b) and trends of SDR over the 50-year period in the middle Yellow River Basin.

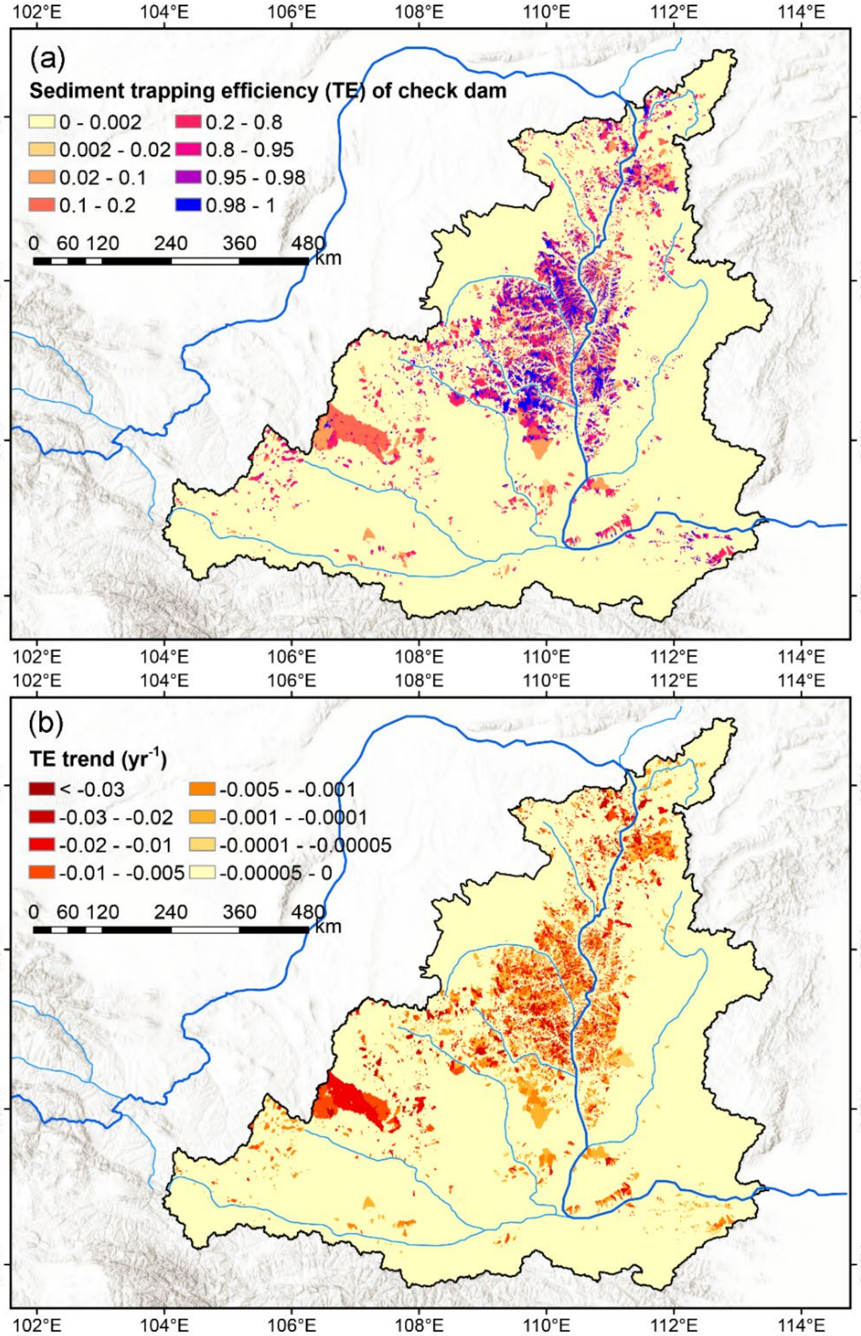

Figure S8. Spatial distribution of (a) average sediment trapping efficiency (TE) of check dams during 1970-2020 and (b) trends of TE over the 50-year period in the middle Yellow River Basin.

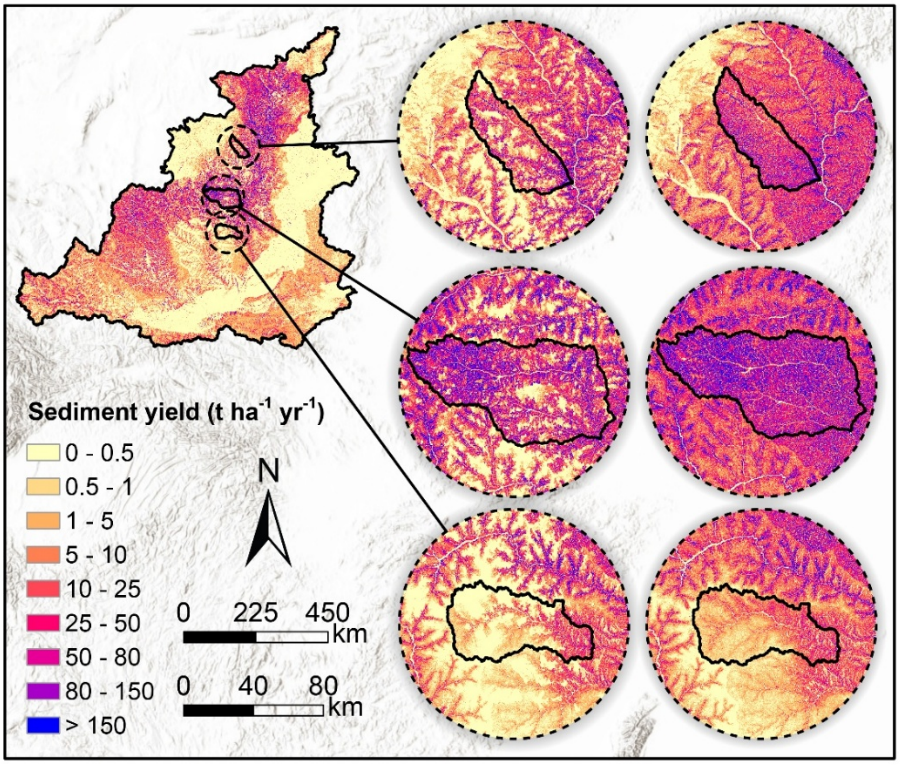

Figure S9. Detailed illustration of the multi-year average sediment yield (SY) incorporating the sediment trapping of check dams in the middle Yellow River Basin. The circular inset on the left provides an enlarged view of the spatial distribution of SY for three selected sub-basins. For comparison, the SY without sediment trapping for the same sub-basin is shown on the right. The upper and lower scale bars represent the main map scale and the enlarged view scale, respectively.

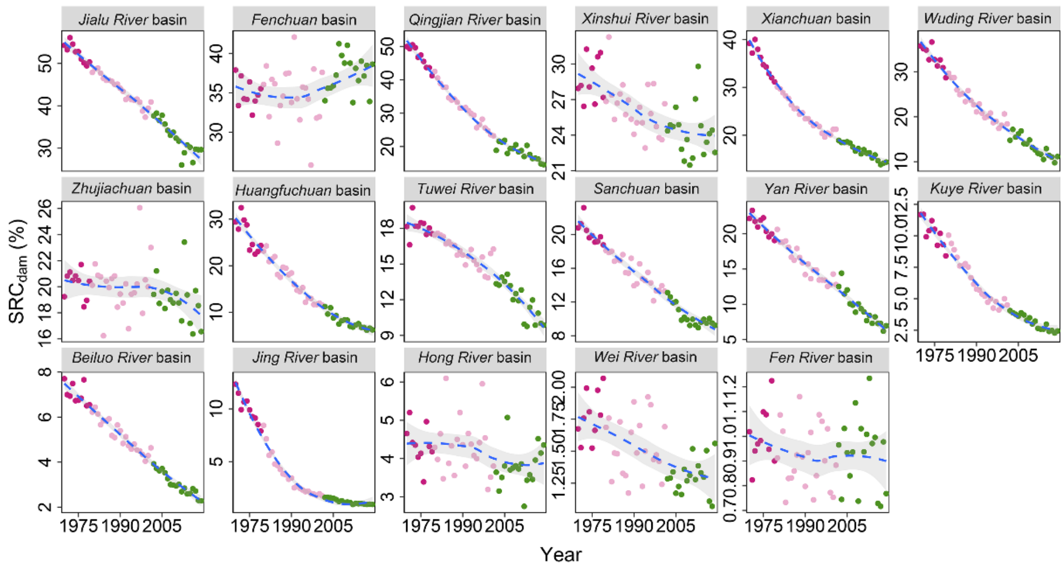

Figure S10. Interannual variation in the sediment reduction contribution by check dams (SRC_{dam}) for the 17 sub-basins in in the middle Yellow River Basin. The three different colors represent sediment yield during 1970-1979, 1980-2001, and 2002-2020.

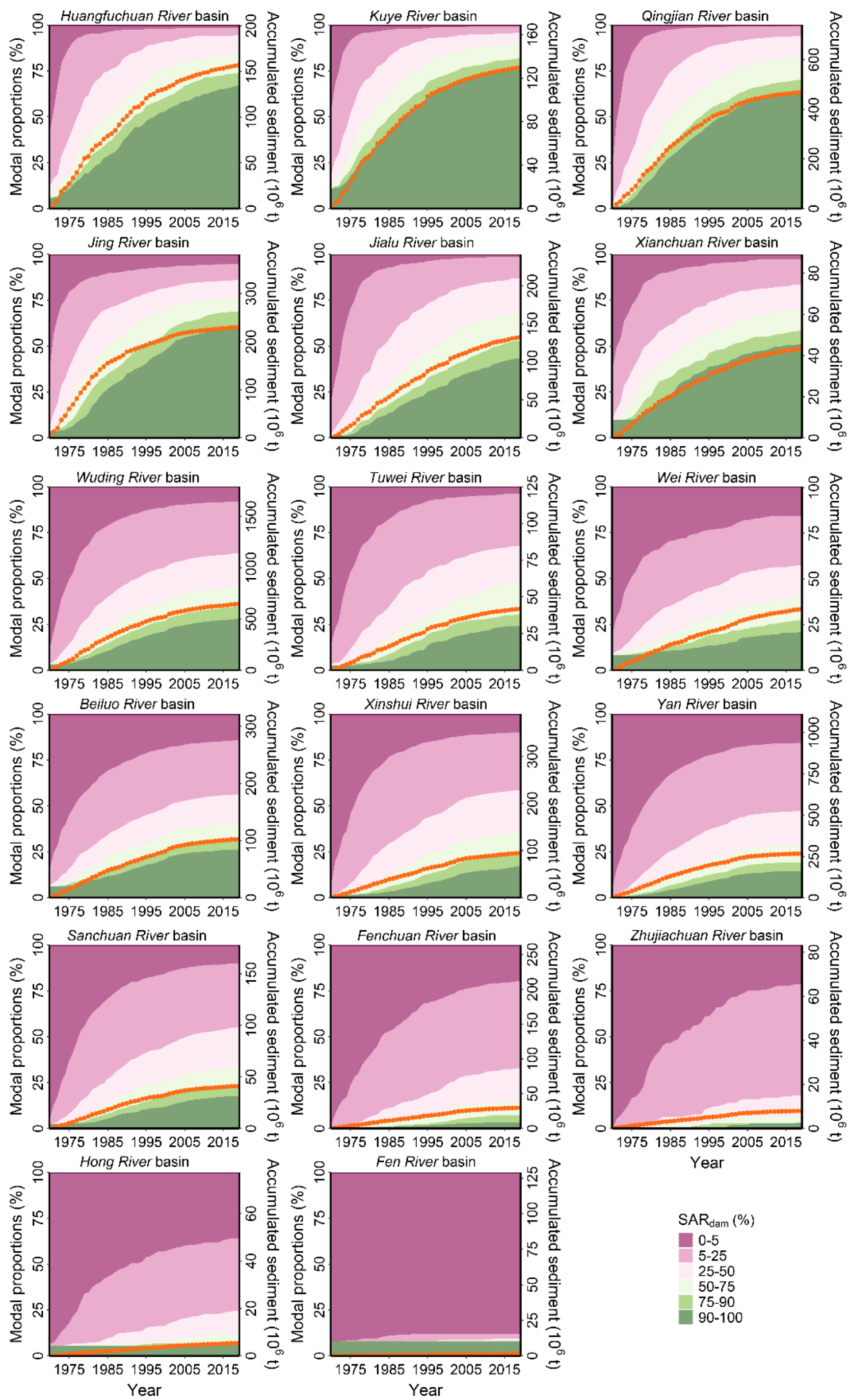

Figure S11. Modal proportions of check dams characterized by different proportions of accumulated sediment relative to total storage capacity (SAR_{dam}) (colored fill), alongside annual changes in accumulated sediment in check dams (orange dotted line) across the 17 sub-basins in the middle Yellow River Basin.

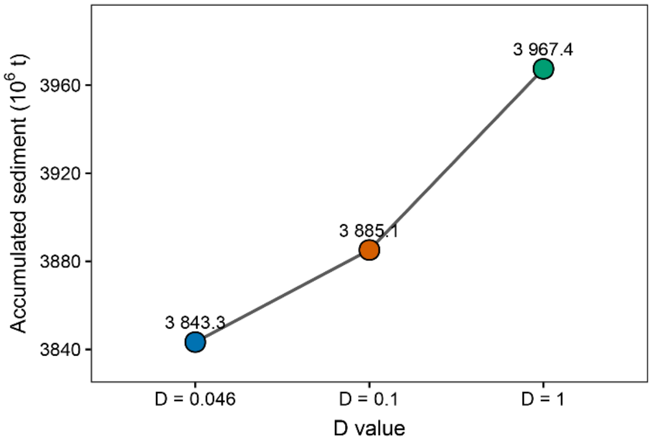

Figure S12. Accumulated sediment under different values of the empirical coefficient *D* in calculating sediment trapping efficiency.

Table S1. Overview of 17 sub-basins controlled by hydrological stations in the middle Yellow River Basin.

No.	Sub-basin	Hydrological station	Area (km^2)	Observed sediment yield ($t\ ha^{-1}\ yr^{-1}$)	Number of check dams
1	Huangfuchuan River	Huangfuchuan	3174.46	55.74	462
2	Kuye River	Wenjiachuan	8651.64	35.99	959
3	Tuwei River	Gaojiachuan	4989.40	14.93	628
4	Jialu River	Shenjiawan	1119.08	35.50	1042
5	Wuding River	Baijiachuan	29622.99	16.25	9471
6	Qingjian River	Yanchuan	3126.31	56.35	2409
7	Yan River	Ganguyi	5817.08	35.91	2157
8	Fenchuan River	Xinshihe	1660.14	10.82	705
9	Zhujiachuan River	Dacun	2139.75	3.04	144
10	Beiluo River	Zhuangtou	25666.54	17.23	1395
11	Jing River	Zhangjiashan	43203.11	26.41	745
12	Wei River	Xianyang	46803.14	8.42	374
13	Hong River	Dangyangqiao	7047.13	5.00	267
14	Xianchuan River	Jiuxian	1562.13	22.51	561
15	Sanchuan River	Houdacheng	4103.75	12.93	918
16	Xinshui River	Daning	3986.84	11.67	1582
17	Fen River	Hejin	38880.22	0.53	441

Table S2. The *P* factor in the RUSLE model based on land use type, slope and terraced distribution.

Land use	Slope/terraces	*P* value
Cropland	0–6°/terraces	0.2
	6–15°	0.35
	15–25°	0.65
	>25°	0.8
Forest and grassland	terraces	0.2
	-	1
Waterbody	-	1
Built land	-	0
Other	-	1